Bull. Mater. Sci., Vol. 40, No. 7, December 2017, pp. 1447–1453
https://doi.org/10.1007/s12034-017-1484-z

Microwave hydrothermal synthesis and upconversion luminescence properties of Yb^{3+}/Tm^{3+} co-doped $NaY(MoO_4)_2$ phosphor

RONG HUANG[1], QI WANG[2], JINSHENG LIAO[2,*] and WEIXIONG YOU[2]
[1]Department of Biochemistry, Ganzhou Teachers College, Ganzhou 341000, China
[2]School of Metallurgical and Chemical Engineering, Jiangxi University of Science and Technology, and Center for Rare-Earth Optoelectronic Materials, Ganzhou 341000, China
*Author for correspondence (jsliao1209@126.com)

MS received 23 October 2016; accepted 1 March 2017; published online 31 October 2017

Abstract. Tetragonal $NaY(MoO_4)_2$ (NYM) phosphors co-doped with Yb^{3+} and Tm^{3+} ions were synthesized through microwave hydrothermal method followed by calcining treatment. Powder X-ray diffraction, Fourier transform infrared spectroscopy, scanning electron microscopy and photoluminescence spectra were used to characterize the properties of as-prepared samples. The results show that Yb^{3+}/Tm^{3+} co-doped NYM displayed bright blue emission near 472 and 476 nm ($^1G_4 \rightarrow {}^3H_6$ transition), strong near-infrared upconversion (UC) emission around 795 nm ($^3H_4 \rightarrow {}^3H_6$ transition). The optimum doping concentrations of Yb^{3+} and Tm^{3+} for the most intense UC luminescence were obtained, and the related UC mechanism of Yb^{3+}/Tm^{3+} co-doped NYM depending on pump power was studied in detail.

Keywords. $NaY(MoO_4)_2$:Yb^{3+}/Tm^{3+}; upconversion luminescence; microwave hydrothermal synthesis.

1. Introduction

Recently, rare-earth (RE)-doped luminescent materials have received extensive attention for their potential applications such as high-resolution displays, phosphors, solid-state lasers, scintillators, communication fibres, optical storage, solar cells and biological fields [1–7]. Among them, upconversion (UC) luminescence from the near-infrared (NIR) region to the visible region, which can convert from lower energy to higher energy radiation through multiple absorption or energy transfer, has been actively studied [8,9]. Trivalent lanthanide ions such as Er^{3+}, Ho^{3+} and Tm^{3+} are commonly used as activator ions for UC luminescence due to their abundant energy levels for radiative transition. In particular, Tm^{3+} is an excellent candidate for a UC luminescent centre because of its unique properties such as blue emission around 480 nm and NIR emission near 800 nm [10,11]. Especially, since the NIR–blue UC process in the Yb- and Tm-co-doped systems requires sequential energy transfer involving at least three photons, its efficiency is generally quite low and such systems are less studied than the Yb- and Er-co-doped systems with higher efficiencies. However, Tm^{3+} has a very low absorption cross-section around 980 nm. Therefore, a sensitizer ion is required to achieve upper level population through energy transfer. Yb^{3+} is usually chosen as the sensitizer in UC materials to facilitate efficient energy transfer from the sensitizer to Tm^{3+} ion, because Yb^{3+} has a large absorption cross-section near 980 nm [12].

To obtain short wavelength lasers, the UC luminescences in fluoride crystals and glasses as well as phosphors have been widely studied during the past several decades due to the low phonon energies of the fluoride compounds [13,14]. However, they are usually unsuitable for practical use due to high production cost, thermal instability and low chemical durability. Instead, crystalline silicates [15], metal oxides [16] and oxide glasses [17] are also continuously explored due to their higher thermal stability and low synthesis cost. Therefore, to explore a novel efficient blue-emitting phosphor applied in NIR is an attractive and challenging research task.

$NaY(MoO_4)_2$ is widely studied as one of the laser host materials for its suitable hardness, high chemical durability and favourable physical properties [18,19]. It is well known that $NaY(MoO_4)_2$ shares scheelite-like ($CaMoO_4$) structure with the tetragonal space group $I4_1/a$, in which Mo^{6+} is coordinated by four oxygen atoms in a tetrahedral site, and the eight RE ions or alkali metal ions are coordinated [20]. The concentration quenching effect hardly occurs in NYM doped with RE ions [21]. Therefore, further exploration of well-controlled shapes and sizes of NYM is still an important research subject.

In this paper, we prepared NYM:Yb^{3+}/Tm^{3+} phosphor by a microwave hydrothermal method. In contrast to the other techniques, the microwave hydrothermal synthesis technique is shown to be promising in the preparation of complex oxides in terms of the rapid processing of materials with cost

reduction, the relatively low reaction temperatures employed, high quality of the crystals obtained. Under excitation into $^2F_{5/2}$ level of Yb^{3+} by 980 nm laser, the blue UC luminescence of NYM:Yb^{3+}/Tm^{3+} phosphor was recorded [22,23]. However, to the best of our knowledge, effect of Tm^{3+} and Yb^{3+} concentrations on blue and NIR UC luminescence from Yb^{3+}/Tm^{3+} co-doped NYM through microwave hydrothermal synthesis has not been studied yet. The UC mechanisms were investigated in detail.

2. Experimental

All chemicals were used as the starting materials without any further purification. $Na_2MoO_4 \cdot 2H_2O$ (AR), Tm_2O_3 (99.99%), Y_2O_3 (99.99%), Yb_2O_3 (99.99%), HNO_3, NaOH (AR) and citric acid were used as raw materials. NYM:Yb^{3+}/Tm^{3+} samples for different Tm^{3+} doping concentrations (0.2–3 at%) with a fixed Yb^{3+} concentration (20 at%) and Yb^{3+} doping concentration (4–30 at%) with a fixed Tm^{3+} concentration (0.5 at%) were prepared by a microwave hydrothermal method. A typical synthesis with 24 at% Yb^{3+}, 0.5 at% Tm^{3+}:$NaY(MoO_4)_2$ is described as follows: 0.0946 g Yb_2O_3, 0.0019 g Tm_2O_3 and 0.1705 g Y_2O_3 were first dissolved in dilute HNO_3 under heating with continuous magnetic stirring. After the Yb_2O_3, Tm_2O_3 and Y_2O_3 were completely dissolved, the excess HNO_3 was removed at the higher temperature. Then, amount of deionized water and 0.4203 g citric acid (metal cation:citric acid = 1:1) were added to obtain $Yb(NO_3)_3$, $Tm(NO_3)_3$ and $Y(NO_3)_3$ mixed solution. Subsequently, 0.9678 g $Na_2MoO_4 \cdot 2H_2O$ was dissolved in a suitable volume of deionized water, then mixed well and slowly added to the above RE nitrate salt solution and a well-controlled amount of NaOH solution was added to the mixed solution with magnetic stirring up to pH 6. After stirring for 1 h, microwave-hydrothermal treatments were conducted at 180°C for 1 h. The time, pressure and power were controlled by a computer. After the synthesis reaction, the product obtained was centrifuged and washed with distilled water and ethanol, and dried at 80°C for 12 h. In the last step, the dried sample was annealed at 600°C for 5 h in air to obtain the white phosphor sample. To investigate the effect of Yb^{3+} and Tm^{3+} contents on the luminescence intensity, the other phosphors with different Yb^{3+}- and Tm^{3+}-doped concentration were synthesized by the same procedure with the corresponding starting materials.

Thermogravimetry (TG) analysis data of the complex precursors were recorded with thermal analysis instrument (Diamond TG), using a sample weight of about 10 mg and a heating rate of 10°C min^{-1} in air atmosphere. X-ray diffractometer (XRD) patterns of samples were examined on a X'Pert PRO (PANalytical) powder diffractometer with CuKα (λ = 0.150465 nm) radiation to identify the crystal phase. Fourier transform infrared spectroscopy (FTIR) measurements were carried out in a Nicolet 5700 FTIR. The morphology of the samples was characterized by a JSM6700F scanning electron microscope (SEM). The UC luminescence spectra and power-dependent properties of sample were obtained using a Fluorolog-3 double monochromator equipped with a Hamamatsu R928 photomultiplier under the excitation of a continuous 980 nm diode laser. All measurements were carried out at room temperature.

3. Results and discussion

3.1 *TG-DTA analysis*

Thermogravimetric differential thermal analysis (TG-DTA) curves of the as-prepared white precursor of the sample NYM:Yb^{3+}/Tm^{3+} are shown in figure 1, where the weight loss occurs in the TG curve up to 600°C with the increase in temperature. Three processes of weight loss occurred in the TG curve from room temperature to 600°C. The first process of weight loss between room temperature and 130°C, the weight loss of 4.9% in TG curve is attributed to the removal of surface absorbed water or the residual water molecules. The second weight loss in the range of 130–300°C is related to the combustion of citric acid and the corresponding weight loss of 2.7% in TG curve. The third step from 300 to 650°C may be related to the decomposition of the residual nitrates. The above processes lead to the total weight loss of 8.7%. No further obvious weight loss was registered above 600°C, which indicates that all the compounds in the precursors are decomposed completely below 600°C. The peaks above three processes of weight loss along with several endothermic and exothermic processes from room temperature to 900°C are found in the DTA curve of figure 1. The strongest exothermic peak at about 570°C represents the formation of the crystallized compound NYM:Yb^{3+}/Tm^{3+} and

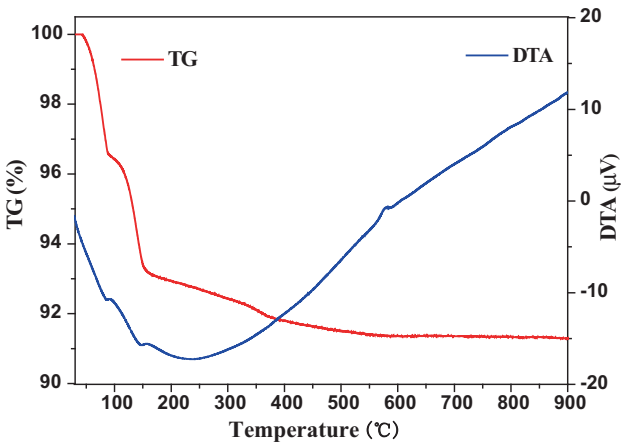

Figure 1. TG-DTA curves of the phosphor NYM:Yb^{3+}/Tm^{3+} precursor in air.

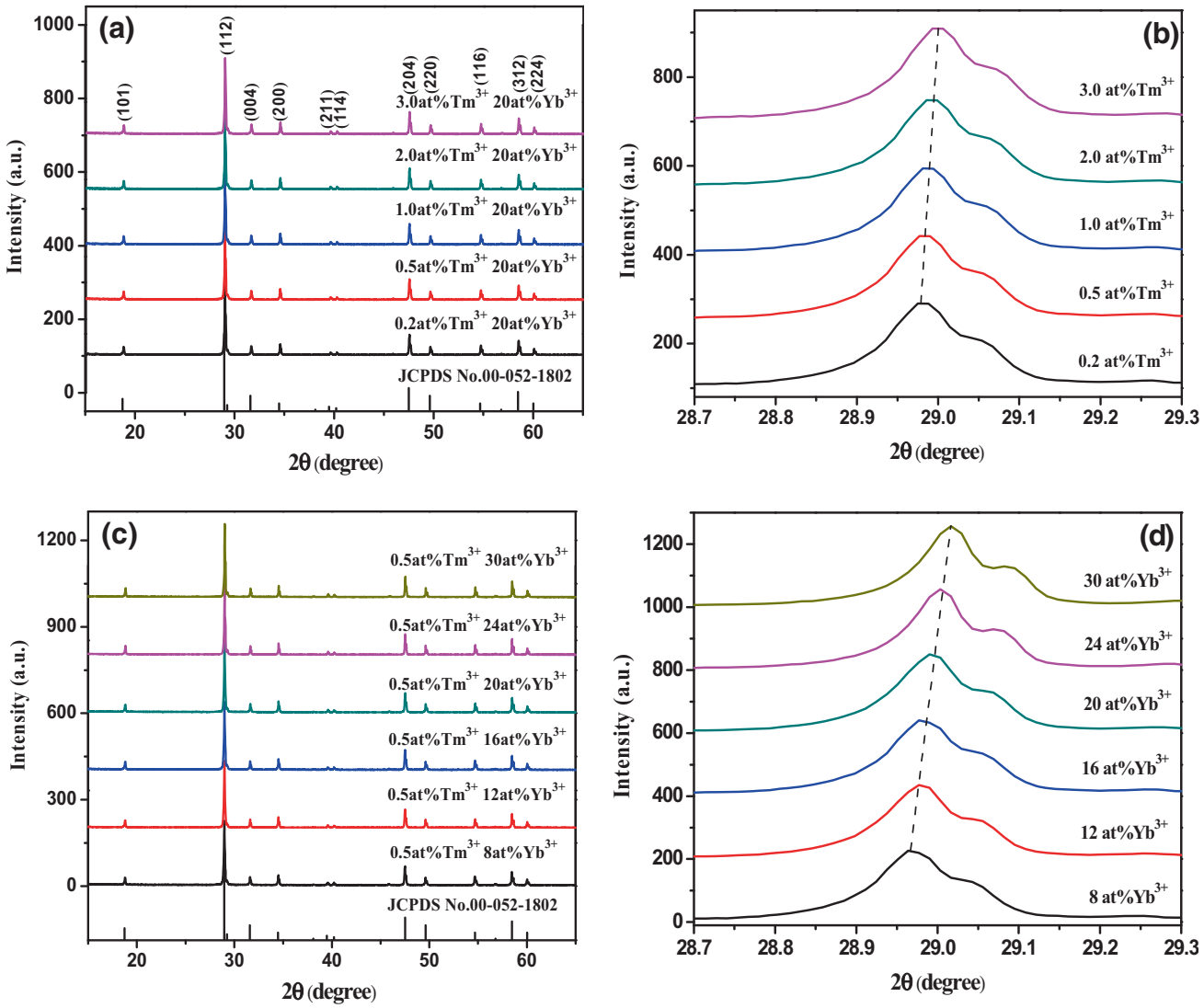

Figure 2. XRD patterns for NYM:Yb^{3+}/Tm^{3+} with (**a**) Tm^{3+} concentration from 0.2 to 3 at% with a fixed 20 at% Yb^{3+}; (**c**) Yb^{3+} concentration from 4 to 30 at% with a fixed 0.5 at% Tm^{3+} samples; (**b** and **d**) enlarged XRD patterns near $2\theta = 29°$ for the (112) peak corresponding to **a** and **c**, respectively. The standard data for $NaY(MoO_4)_2$ (JCPDS no. 052-1802) is also presented in the figure.

when the temperature reaches 600°C, it was crystallized very well.

3.2 *Structure and morphology of NYM:Yb^{3+}/Tm^{3+}*

The phase composition and purity of the NYM:Yb^{3+}/Tm^{3+} product obtained by microwave hydrothermal method with further sintering treatment were examined by XRD technique. Figure 2 shows XRD patterns of the Yb^{3+}/Tm^{3+}-co-doped NYM sample for (a) various Tm^{3+} concentrations up to 3 at% with a fixed 20 at% Yb^{3+} and (c) various Yb^{3+} concentrations up to 30 at% with a fixed 0.5 at% Tm^{3+}. The peak positions agree well with those of the standard diffraction pattern of tetragonal $NaY(MoO_4)_2$ (JCPDS no. 052-1802). However, with increasing Yb^{3+} (Tm^{3+}) concentration, the diffraction peaks of 2θ were shifted to a higher angle, illustrating substitution of Yb^{3+} (Tm^{3+}) ions with Y^{3+} ion sites and the resultant shrinkage of lattice constants (figure 2b and d). It is noted that the diffraction peak (112) of NYM:Yb^{3+}/Tm^{3+} samples is slightly shifted to the higher-angle, but do not change $NaY(MoO_4)_2$ crystal structure. Because, Yb^{3+}, Tm^{3+} and Y^{3+} are RE ions, which have similar ionic radius and the same valence, even if Tm^{3+} and Yb^{3+} are under high doping concentration, the radii of Yb^{3+} (0.0868 nm, CN = 6) and Tm^{3+} (0.0880 nm, CN = 6) are slightly smaller than that of Y^{3+} (0.0900 nm, CN = 6), Yb^{3+} and Tm^{3+} can be easily doped into host lattice and substituted for the site of Y^{3+} ions. We conclude that Yb^{3+} and Tm^{3+} were efficiently incorporated into the host lattice of NYM crystal. SEM image (figure 3) showed the morphology as rice-like shape and the particle size is about 500 nm in length and 150 nm in width.

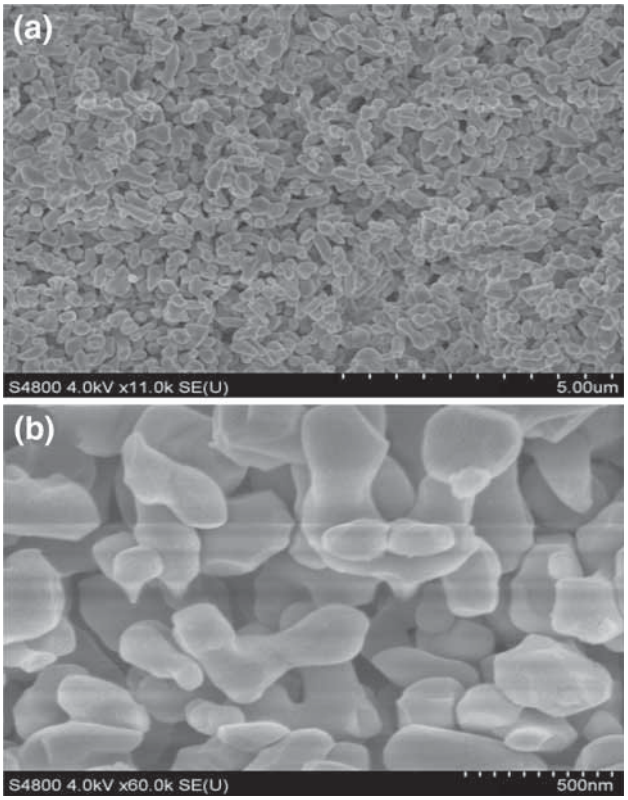

Figure 3. (**a**) Low- and (**b**) high-magnifications of SEM image of the NYM:24 at% Yb^{3+}/0.5 at% Tm^{3+} sample.

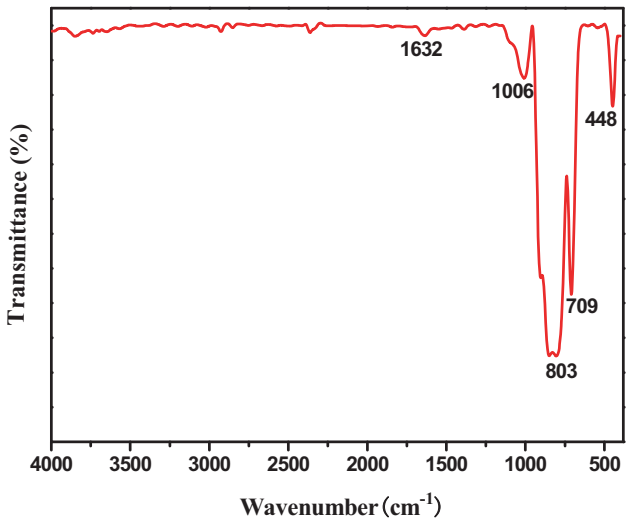

Figure 4. FTIR spectra of NYM:24 at% Yb^{3+}/0.5 at% Tm^{3+} sample.

3.3 *FTIR spectral analysis*

It is well known that FTIR is a unique tool used to identify the functional groups and frequency of vibration between the bonds with the atoms in the crystal lattice. Figure 4 shows the FTIR transmittance spectrum of NYM:24 at% Yb^{3+}/0.5 at% Tm^{3+} sample obtained in the range of 400–4000 cm^{-1}. Marques *et al* [24] reported that for tetrahedral symmetry, $F_2(\nu_3)$ modes of vibrations are IR active [24]. Our results show that the strong absorption bands at 803 and 709 cm^{-1} are related to the stretching vibrations of O–Mo–O in the MoO_4^{2-} tetrahedron [25]. The peak at 448 cm^{-1} is due to O–Mo–O in-plane bending vibration. These absorption bands were assigned to the antisymmetric stretch $F_2(\nu_3)$ of the scheelite tetragonal crystalline structure. The peak at 1006 cm^{-1} is attributed to the adsorption of the carboxylate group on the surface of the NYM:Yb^{3+}/Tm^{3+} microstructures [26]. The weak absorption at 1632 cm^{-1} is assigned to O–H bending vibration of the absorbed water from air [27].

3.4 *UC luminescence properties*

To investigate concentration quenching of Yb^{3+}/Tm^{3+} co-doped NYM, figure 5a and b shows the dependence of the UC luminescence spectra of the Yb^{3+}/Tm^{3+} co-doped NYM phosphors on the sensitizer (Yb^{3+}) and activator (Tm^{3+}) concentrations, respectively. As shown in figure 5a, at a fixed Yb^{3+} concentration (20 at%), the intensities of all emission regions were increased with increased Tm^{3+} concentration up to 0.5 at%, and then decreased at concentrations over 0.5 at%. Moreover, as shown in figure 5b, at a fixed Tm^{3+} concentration (20 at%), with increasing Yb^{3+} concentrations up to 24 at%, the intensities of all emission regions increased, while emission intensities declined at concentrations over 24 at% due to a quenching effect [28]. This concentration quenching effect could be explained by the energy transfer between the nearest dopant (Yb^{3+} and Tm^{3+}) ions. As dopant ion concentrations are increased, the distance between dopant ions shrinks, allowing non-radiative energy transfer such as exchange or multipole–multipole interactions. On account of our results, we concluded that the optimum Yb^{3+}/Tm^{3+} doping concentrations were 24/0.5 at% (summarized in the inset of figure 5a and b). The UC emissions in Yb^{3+}/Tm^{3+} co-doped NYM were dominated by strong blue and NIR emissions, while red emission was weaker than blue and NIR emissions. The UC luminescent spectra of Yb^{3+}/Tm^{3+} co-doped NYM consists the following three regions: (1) bright blue emissions near 472 and 476 nm generated by the $^1G_4 \rightarrow {}^3H_6$ transition; (2) relatively weak red emission near 648 nm due to the $^3F_2 \rightarrow {}^3H_6$ and $^1G_4 \rightarrow {}^3F_4$ transitions; and (3) strong NIR UC emission around 795 nm attributed to the $^3H_4 \rightarrow {}^3H_6$ transition.

Figure 6 shows the blue, red and NIR intensities of NYM co-doped with Tm^{3+}/Yb^{3+} (24/0.5 at%) in a logarithmic diagram as a function of pump power. The emission intensity I_{em} depends on the excitation power I_P, following the relationship of $I_{em} \propto (I_P)^n$, where n is the number of the pumping photons required to excite RE ions from the ground state to the emitting excited state. The calculated results indicated that the slopes of the n values were 2.68, 1.61 and 1.68 for blue, red and NIR emissions, respectively. The n value for

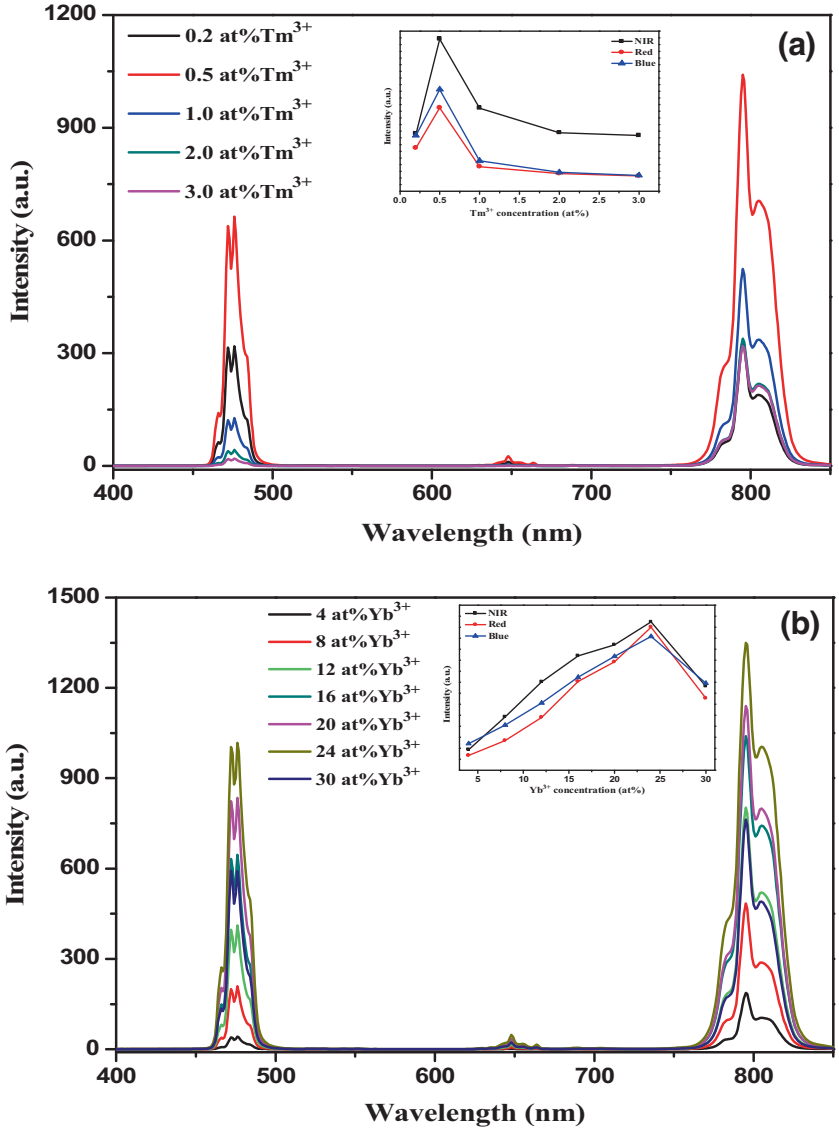

Figure 5. UC emission spectra of the NYM:Yb^{3+}/Tm^{3+} samples for (**a**) different Tm^{3+} concentrations with a fixed 20 at% Yb^{3+} and (**b**) different Yb^{3+} concentrations with a fixed 0.5 at% Tm^{3+} under 980 nm excitation.

blue emission ($^1G_4 \rightarrow {}^3H_6$) was over 2 and close to 3, while that for red emission ($^3F_2 \rightarrow {}^3H_6$ and $^1G_4 \rightarrow {}^3F_4$) and NIR ($^3H_4 \rightarrow {}^3H_6$) were < 2. This result implies that the UC mechanism corresponding to blue emission can be explained by a three-photon process, while red and NIR emissions can be induced by a two-photon process.

Figure 7 illustrates the energy level diagrams with transitions which may be involved in the energy transfer process between Yb^{3+} and Tm^{3+} in NYM:Yb^{3+}/Tm^{3+} nanophosphors. Under excitation at 980 nm, non-resonant energy transfer occurs from the $^2F_{5/2}$ state in the Yb^{3+} to the $^3H_5$ level in the Tm^{3+} and (or) ground state absorption (GSA) process by a $^3H_6 \rightarrow {}^3H_5$ transition. Then, $^3H_5 \rightarrow {}^3F_4$ transition can be generated by non-radiative relaxation. The $^3F_2$ state can then be excited from the $^3F_4$ state through excited state absorption (ESA) or energy transfer UC (ETU) generating the metastable $^3H_4$ state from a non-radiative transition, which plays an important role in the generation of blue and NIR emissions [29]. For blue emission, the $^3H_4$ state can be further excited to the $^1G_4$ state through ESA or ETU. Finally, the $^1G_4 \rightarrow {}^3H_6$ transition generates the blue emission centre. The red emission is attributed to the $^3F_2 \rightarrow {}^3H_6$ transition. For NIR emission, the metastable $^3H_4$ state that is not excited to the high energy state in Tm^{3+}, such as the $^1G_4$ state, generates the NIR emission by radiative transition of $^3H_4 \rightarrow {}^3H_6$. The $^3F_2$ state can be populated only by the $^3H_5 \rightarrow {}^3F_2$ transition by ESA and ETU processes. According to the energy gap law, the non-radiative transition of $^3H_5 \rightarrow {}^3F_4$ dominates

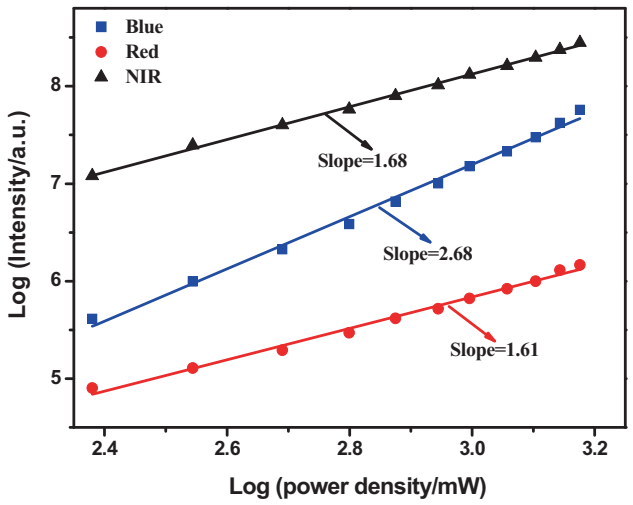

Figure 6. Dependences of the upconversion intensities (I_{em}) for transition bands on the 980 nm pumping laser power (I_p) at blue, red and NIR intensities of $NaY(MoO_4)_2$ co-doped with Yb^{3+}/Tm^{3+} (24/0.5 at%).

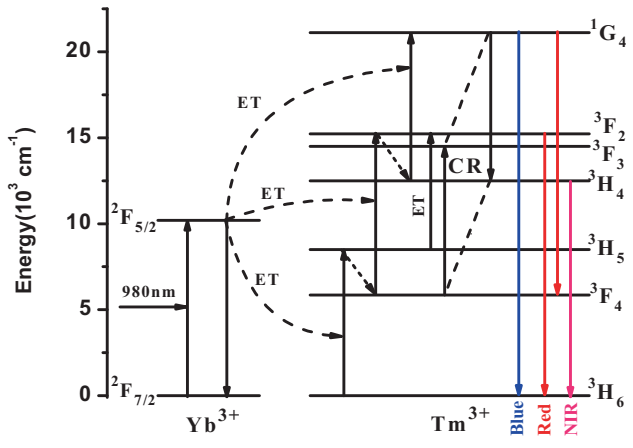

Figure 7. Energy level diagrams of Yb^{3+} and Tm^{3+} ions and upconversion emission mechanism in NYM:Yb^{3+}/Tm^{3+}.

rather than the $^3H_5 \rightarrow {}^3F_2$ transition, because the energy gap between the $^3H_5$ and $^3F_4$ states is too small [30]. Therefore, the $^3F_2$ state cannot be populated well, thus, generating the weak red emission. Moreover, the intensity of the NIR emission is higher than that of the blue emission. This might be due to the increased population of the $^3H_4$ state [31]. The energy gap between $^1G_4$ and $^3H_4$ is smaller than that is between $^3F_4$ and $^3F_2$ (740 cm^{-1}) [32]. Therefore, through the CR process, the energy transition of $^1G_4 \rightarrow {}^3H_4$ can easily populate the $^3F_3$ state instead of the $^3F_2$ state. Moreover, the $^3F_3$ state can easily relax to the $^3H_4$ state because the energy gap between $^3F_3$ and $^3H_4$ is too small, which can increase the population of the $^3H_4$ state and the radiative transition of $^3H_4 \rightarrow {}^3H_6$.

4. Conclusion

In summary, the tetragonal Yb^{3+}/Tm^{3+} co-doped NYM phosphors with different Yb^{3+} (Tm^{3+}) doping concentrations were synthesized by microwave hydrothermal method. The Yb^{3+}/Tm^{3+} co-doped NYM phosphor has strong blue and NIR luminescent centres at 472 and 476 nm ($^1G_4 \rightarrow {}^3H_6$), and 795 nm ($^3H_4 \rightarrow {}^3H_6$), respectively, while it has a very weak red emission centre around 648 nm ($^3F_2 \rightarrow {}^3H_6$) under 980 nm excitation. The optimal concentrations of Yb^{3+} and Tm^{3+} ions are about 24 and 0.5 at%, respectively. Power-dependent study reveals that blue emission ($^1G_4 \rightarrow {}^3H_6$) arises from a three-photon process, while strong NIR ($^3H_4 \rightarrow {}^3H_6$) and weak red emission ($^3F_2 \rightarrow {}^3H_6$) are dominated by a two-photon process. Based on our results and analysis, we conclude that Yb^{3+}/Tm^{3+} co-doped NYM is an excellent candidate for blue and NIR UC phosphors.

Acknowledgements

This work was financially supported by the National Natural Science Foundation of China (No. 51162012) and the Science Program of the Education Office, Jiangxi Province (No. GJJ160597) and the Major Project of Natural Science Foundation of Jiangxi Province (No. 20165ABC28010).

References

[1] Zhou L, Wang R, Yao C, Li X M, Wang C L, Zhang X Y *et al* 2015 *Nat. Commun.* **6** 6938
[2] Li P, Peng Q and Li Y 2009 *Adv. Mater.* **21** 1945
[3] Zhou J, Liu Q, Feng W, Sun Y and Li F Y 2014 *Chem. Rev.* **115** 395
[4] Luo W Q, Wu H Y and Li B 2016 *Chem. Phys. Lett.* **658** 215
[5] Tian G, Gu Z J, Zhou L J, Yin W Y, Liu X X, Yan L *et al* 2012 *Adv. Mater.* **24** 1226
[6] Dissanayake K T and Rabuffetti F A 2016 *J. Mater. Chem. C* **4** 2447
[7] Urbina-Frías A, López-Luke T, Oliva J, Salas P, Torres-Castro A and De la Rosa E 2016 *J. Lumin.* **172** 154
[8] Vetrone F, Mahalingam V and Capobianco J A 2009 *Chem. Mater.* **21** 1847
[9] Cao C, Qin W, Zhang J, Wang Y, Wang G, Wei G *et al* 2008 *Opt. Commun.* **281** 1716
[10] Suyver J F, Grimin J, Van Veen M K, Biner D, Kramer K W and Gudel H U 2006 *J. Lumin.* **117** 1
[11] Zhang Q Y, Li T, Jiang Z H, Ji X H and Buddhudu B 2005 *Appl. Phys. Lett.* **87** 1911
[12] Gapontsev V P, Matitsin S M, Isineev A A and Kravcheko V B 1982 *Opt. Laser Technol.* **14** 189
[13] Chen D Q, Wang Y S, Yu Y L and Huang P 2007 *Appl. Phys. Lett.* **91** 051920
[14] Owen J J, Cheetham A K and Mcfarlane R A 1998 *J. Opt. Soc. Am. B* **15** 684
[15] Rakov N, Maciel G S, Guimaraes R B and Carvalho I C S 2010 *Mater. Chem. Phys.* **123** 199

[16] Sun Q, Zhao H, Chen X Q, Wang P F, Cai W and Jiang Z H 2010 *Mater. Chem. Phys.* **123** 806
[17] Su F N and Deng Z D 2007 *Opt. Mater.* **29** 1452
[18] Huang Y, Zhou L, Yang L and Tang Z 2011 *Opt. Mater.* **33** 777
[19] Kaminskii A, Agamalyan N, Kozeeva L, Nesterenko V and Pavlyuk A 1983 *Phys. Status Solidi A* **75** K1
[20] Yan B and Wu J H 2009 *Mater. Chem. Phys.* **116** 67
[21] Wu J and Yan B 2010 *J. Am. Ceram. Soc.* **93** 2188
[22] Li Y, Wang G F, Pan K, Zhou W, Wang C, Fan N Y *et al* 2012 *CrystEngComm.* **14** 5015
[23] Li Y, Wang G F, Pan K, Qu Y, Liu S and Feng L 2013 *Dalton Trans.* **42** 3366
[24] Marques A P A, Motta F V, Cruz M A, Varela J A, Longo E and Rosa I L V 2011 *Solid State Ionics* **202** 54
[25] Frost R L, Cejka J and Dickfos M J 2008 *J. Raman Spectrosc.* **39** 779
[26] Bu W B, Chen Z X, Chen F and Shi J L 2009 *J. Phys. Chem. C* **113** 12176
[27] Neera S J, Kijima N and Cheetham A K 2004 *Chem. Phys. Lett.* **387** 2
[28] Yang D M, Li C X, Li G G, Shang M M, Kang X J and Lin J 2011 *J. Mater. Chem.* **21** 5923
[29] Etchart I, Hernandez I, Huignard A, Berard M, Laroche M, Gillin W P *et al* 2011 *J. Appl. Phys.* **109** 063104
[30] Chung J H, Lee S Y, Shim K B, Kweon S Y, Ur S C and Ryu J H 2012 *Appl. Phys. A* **108** 369
[31] Wang F and Liu X G 2008 *J. Am. Chem. Soc.* **130** 5642
[32] Mishra K, Girl N K and Rai S B 2011 *Appl. Phys. B* **103** 863